DNA-protein binding rates: Bending fluctuation and hydrodynamic coupling effects

Yann von Hansen,[1] Roland R. Netz,[1,a)] and Michael Hinczewski[1,2]

[1]*Department of Physics, Technical University of Munich, 85748 Garching, Germany*
[2]*Institute for Physical Science and Technology, University of Maryland, College Park, Maryland 20742, USA*

We investigate diffusion-limited reactions between a diffusing particle and a target site on a semiflexible polymer, a key factor determining the kinetics of DNA-protein binding and polymerization of cytoskeletal filaments. Our theory focuses on two competing effects: polymer shape fluctuations, which speed up association, and the hydrodynamic coupling between the diffusing particle and the chain, which slows down association. Polymer bending fluctuations are described using a mean field dynamical theory, while the hydrodynamic coupling between polymer and particle is incorporated through a simple heuristic approximation. We validate both of these through comparison to Brownian dynamics simulations. Neither of the effects has been fully considered before in the biophysical context and we show they are necessary to form accurate estimates of reaction processes. The association rate depends on the stiffness of the polymer and the particle size, exhibiting a maximum for intermediate persistence length and a minimum for intermediate particle radius. In the parameter range relevant to DNA-protein binding, the rate increase is up to 100% compared with the Smoluchowski result for simple center-of-mass motion. The quantitative predictions made by the theory can be tested experimentally. © *2010 American Institute of Physics*. [doi:10.1063/1.3352571]

I. INTRODUCTION

Reactions between semiflexible polymers and small molecules are ubiquitous in cells, playing a crucial role in a large number of biological processes: examples include the interaction of gene-regulating proteins with specific target sites on DNA, and the polymerization of DNA or structural proteins such as actin and tubulin. Many of these reactions are diffusion-limited[1]—the activation free-energy is negligible compared with the thermal energy k_BT and the reaction is not hindered by other steric or conformational factors—so the overall association speed therefore depends on the rate at which the reactive molecules approach each other.

DNA-protein interaction has been the most widely studied process of this type,[2,3] attracting attention since the first measurement of the reaction rate between the *lac* repressor and operator[4] revealed that it far exceeds the three-dimensional (3D) diffusion limit. The quest to identify the underlying mechanism culminated in the seminal idea of facilitated diffusion by Berg, Winter, and von Hippel[5–7] but the general description of DNA-protein interaction is still far from complete. Although recent single molecule experiments show evidence that certain proteins indeed make use of facilitated diffusion,[8,9] the majority of measured reaction rates for DNA-binding proteins[2,10,11] do not exceed the Smoluchowski result for 3D diffusion.[12] Thus, recent years have seen extensive theoretical efforts[13–17] revisiting the underlying assumptions of facilitated diffusion, and examining it anew in response to experimental advances.

Diffusion-controlled reactions with targets on flexible polymers are a well-established subject in polymer physics, with general analytical frameworks developed by Wilemski and Fixman,[18,19] and Szabo, Schulten, and Schulten[20] decades ago. Using the Wilemski–Fixman approach and a Gaussian model for circular polymers, a study by Berg looked at the influence of internal DNA motion on the binding of proteins.[21] However, little is known about the role of chain stiffness, and both Berg's study and the classic polymer reaction rate theories do not include hydrodynamics. This is a significant oversight, because solvent-mediated interactions modify not only the approach of the particle to the target site but also the fluctuation of the entire polymer contour, and thus all time scales involved in the dynamics. Moreover, the two effects are in opposition: polymer fluctuations lead to the target site exploring a larger configurational space than simple center-of-mass diffusion and hence the association rate is enhanced; the hydrodynamic coupling between the particle and coil, on the other hand, reduces their relative mobility, decreasing the rate. The observed binding rate is a subtle competition between these two phenomena. As experiments are providing an ever more detailed picture of biological reactions at the single molecule level, we need theories that begin to grapple with the full complexity of polymer-particle diffusive motion.

The paper is organized as follows: in Sec. II, we briefly review the renewal approach used to derive first passage times and association rates in the diffusion-controlled limit; a

discussion of a few effects going beyond this limit is contained in Appendix A . The theoretical analysis of the dynamics in the polymer-particle system makes use of a mean field approach for the polymer dynamics and a heuristic approximation for interparticle hydrodynamics. The main results are shown in Sec. II, while a brief review of the theory and calculational details are postponed to the Appendixes B and C. The Brownian dynamics (BD) simulation method used to independently test the theoretical description is described in Sec. III. The detailed validation of the theory through BD simulation results is presented in Sec. IV. We then investigate how the mechanical characteristics of the semiflexible polymer—the contour and persistence lengths—affect the reaction rate. Ultimately our theory yields quantitative predictions that can be tested empirically. Section V summarizes the main results and offers suggestions for future experiments.

II. THEORY

A. Diffusion-controlled reaction rates

In general, association rates are calculated by finding the steady-state solution of a diffusion equation with absorbing boundary conditions.[22,23] In our case, we can employ the simpler renewal approach,[24,25] which avoids the necessity of imposing absorbing boundaries: first passage times and binding rates can be directly extracted from the solution of the unbounded problem, i.e., the dynamic Green's function describing the time evolution of the relative distance between reactants subject to diffusive motion. The renewal approach is in principle equivalent to the Wilemski–Fixman formalism, and they share the same underlying approximations:[26,27] (i) the Green's function for the time evolution of the particle-target distance is assumed to be that of a stationary Markov process; (ii) excluded-volume between the reactants is ignored. In the following, we briefly review the main aspects of the approach.

For a stochastic process in one dimension, the Green's function $g(x, x_0; t)$ specifies the probability to find the particle at x at time t given a starting point x_0 at time $t=0$. If we are interested in paths that reach a boundary point x_a in time t, the corresponding transition probability can be written as a convolution,

$$g(x_a, x_0; t) = \int_0^t dt' f(t'; x_a, x_0) g(x_a, x_a; t - t'), \tag{1}$$

where $f(t; x_a, x_0)$ is the first passage time distribution: the probability of reaching x_a in time t starting from x_0 at $t=0$ without passing through x_a along the way. A Laplace transformation $\mathcal{L}$ acting on the time variable t leads to

$$\tilde{g}(x_a, x_0; s) = \tilde{f}(s; x_a, x_0) \tilde{g}(x_a, x_a; s)$$

$$\Leftrightarrow \quad f(t; x_a, x_0) = \mathcal{L}^{-1} \left[\frac{\tilde{g}(x_a, x_0; s)}{\tilde{g}(x_a, x_a; s)} \right], \tag{2}$$

where Laplace transforms are denoted by $\mathcal{L}[f(t)] = \tilde{f}(s)$. Note that $g(x, x_0; t)$ is the Green's function in the absence of ab-

sorbing boundary conditions; we assume only that the probability vanishes at $x \to \pm \infty$.

To investigate the role of polymer fluctuations and of hydrodynamics on the reaction rates of diffusion controlled reactions, we consider an idealized situation: the only parameter relevant for the binding process then is the radial distance r between the reactants, meaning that the problem is effectively reduced to one dimension. Deviations from this simple picture and their impact on the association rates are discussed in Appendix A. In the case of perfect absorption, particles bind when they collide for the first time—when the relative distance r reaches the absorption radius r_a. As a result, the binding rate $k_a(t)$ can be obtained from the first passage time distribution by integrating over all possible initial separations

$$k_a(t) = 4\pi \int_{r_a}^{\infty} dr_0 r_0^2 f(t; r_a, r_0). \tag{3}$$

The steady-state rate k_a reached at long times is extracted from the Laplace transform $\tilde{k}_a(s)$ using the final value theorem

$$k_a = \lim_{t \to \infty} k_a(t) = \lim_{s \to 0} s\tilde{k}_a(s). \tag{4}$$

For the simple case of two kinds of uncoupled Brownian particles with diffusion constants D_1 and D_2, the radial Green's function, which will explicitly be shown in Sec. II B [Eqs. (10) and (11)], can be easily written down and the result for the first passage time distribution in Laplace space reads

$$\tilde{f}(s; r_a, r_0) = \frac{r_a}{r_0} \exp\left(-(r_0 - r_a)\sqrt{\frac{s}{D}}\right), \tag{5}$$

with total diffusion constant $D = D_1 + D_2$. Applying Eq. (3), which corresponds to imposing uniform initial concentrations at time $t=0$, one obtains the association rate

$$k_a(t) = 4\pi D r_a \left(1 + \frac{r_a}{\sqrt{\pi D t}}\right), \tag{6}$$

which at long times reduces to the well-known Smoluchowski rate[12] $k_S = 4\pi D r_a$ constituting the upper limit for reaction rates governed by Brownian diffusion in three dimensions.

For the more complicated polymer-particle case, the renewal method works analogously, but the Laplace transforms must be carried out numerically using standard numerical techniques:[28] the Laplace transformation of the numerator in Eq. (2) is performed with the routine *gsl_integration_qags* with upper integration boundary $50/s$, while the Laplace transform of the denominator in Eq. (2) and the numerical integration over initial separations r_0 in Eq. (3) are obtained using the routine *gsl_integration_qagiu*; a workspace of 10^5 intervals was allocated for all these routines and the relative and absolute error bounds were set to 10^{-7}. For the numerical implementation of the final value theorem in Eq. (4) the values $s \approx 1-2 \times 10^{-8} \tau^{-1}$ ($\tau \equiv 6\pi \eta a^3/k_B T$ being the diffusional time scale of a spherical particle of radius a in a solvent of viscosity η) proved appropriate: within this range the nu-

merical evaluation of the steady state Smoluchowski rate k_S coincided with the analytic result within a typical relative accuracy of $\lesssim 10^{-5}$. Results of the renewal approach applied to DNA-protein dynamics are presented in Sec. IV.

B. Dynamic Green's functions

As outlined above, the knowledge of dynamic Green's functions specifying the probability that a radial distance r between two objects is realized at time t after starting at a radial distance r_0 allows the calculation of association rates. The first step toward the description of the polymer-particle system consists in the analysis of the polymer motion itself: The dynamics of semiflexible polymers including hydrodynamics can be captured by a mean field theory (MFT) discussed in detail in Ref. 29, where the model was shown to provide an accurate description of internal polymer kinetics, validated through extensive comparisons with BD simulations. Moreover, the theory can be independently tested by comparison with recent fluorescence correlation spectroscopy experiments:[30] without any fitting parameters, it exhibits excellent agreement for the mean square displacement (MSD) of tagged ends of single dsDNA fragments diffusing in solution.[31]

Here we demonstrate that the mean field approach in addition also exhibits excellent agreement for the dynamic Green's function characterizing the motion of specific points on the polymer contour when comparing theory and BD results. A short overview of the theory and details concerning the derivation can be found in Appendix B; the result of the calculation involving a normal mode expansion is a Gaussian Green's function specifying the conditional probability that a point on the polymer contour (specified by the arc-length variable s) reaches spatial position $\mathbf{r}$ in time t given a start at $\mathbf{r}_0$,

$$G(\mathbf{r},\mathbf{r}_0;t) = (2\pi V(t))^{-3/2}\exp\left(-\frac{(\mathbf{r}-\mathbf{r}_0)^2}{2V(t)}\right), \tag{7}$$

$$V(t) = 2D_{\text{pol}}t + 2k_BT\sum_{n=1}^{N}\frac{\Theta_n}{\Lambda_n}(1-e^{-\Lambda_n t})\Psi_n(s)^2. \tag{8}$$

In Eq. (8) D_{pol} denotes the center-of-mass diffusion constant of the polymer coil and is given in Appendix B. The values of the fluctuation dissipation parameters Θ_n and of the inverse relaxation times Λ_n result from the (numerical) evaluation of the hydrodynamic interaction tensor; the normal modes $\Psi_n(s)$ with mode number n additionally depend on polymer parameters, i.e., contour length L and persistence length l_p. The variance $V(t)$ in Eq. (8) thus has contributions of the center-of-mass motion of the entire polymer coil and of internal fluctuations of the contour: on large time scales $t \gg \Lambda_1^{-1}$ the variance reduces to $V(t) \approx 2D_{\text{pol}}t$ and hence the motion is dominated by the Brownian diffusion of the polymer's center-of-mass, for smaller times, however, the contribution from internal polymer modes becomes important. The radial Green's function $G_{\text{rad}}(r;t)$ for a particle starting at $\mathbf{r}_0 = 0$ is obtained by integrating $G(\mathbf{r},0;t)$ over the surface of a sphere of radius r,

$$G_{\text{rad}}(r;t) = \frac{4\pi r^2}{(2\pi V(t))^{3/2}}\exp\left(-\frac{r^2}{2V(t)}\right). \tag{9}$$

In Sec. IV, we compare the time evolution of this transition probability for the case of the end-monomer ($s = \pm L/2$) to BD simulation results.

Hydrodynamic interactions influence the relative motion of diffusing objects: these interactions are included in our analytic approach by a heuristic approximation, which is motivated for the case of two spherical particles and for the case of a single diffusing particle and a specific target site on a polymer in Appendix C.

In general, the dynamic Green's function takes the form of a Gaussian centered at the initial separation $\mathbf{r}_0$; the integration over a sphere of radius $r = |\mathbf{r}|$ leads to the radial Green's function

$$G_{\text{rad}}^{\alpha}(r,r_0;t) = \frac{r}{r_0\sqrt{2\pi V^{\alpha}(t)}}\left[\exp\left(-\frac{(r-r_0)^2}{2V^{\alpha}(t)}\right) - \exp\left(-\frac{(r+r_0)^2}{2V^{\alpha}(t)}\right)\right], \tag{10}$$

where the superscript $\alpha = n, h$ discriminates between radial Green's functions without and with hydrodynamics. In total, we distinguish four cases in our analysis: two spherical particles without hydrodynamics (i) and with hydrodynamics (ii), and a spherical particle and a specific target point on a semiflexible polymer without hydrodynamics (iii) and with hydrodynamics (iv), for which the respective variances are as follows:

$$\text{(i)} \quad V^n(t) = 2(D_1 + D_2)t, \tag{11}$$

$$\text{(ii)} \quad V^h(t,r_0) = 2(D_1 + D_2 - 2\bar{\chi}(r_0,t))t, \tag{12}$$

$$\text{(iii)} \quad V^n(t) = 2D_{\text{par}}t + 2D_{\text{pol}}t + 2k_BT\sum_{n=1}^{N}\frac{\Theta_n}{\Lambda_n} \times (1-e^{-\Lambda_n t})\Psi_n(s)^2, \tag{13}$$

$$\text{(iv)} \quad V^h(t,r_0) = 2D_{\text{par}}t + 2D_{\text{pol}}t + 2k_BT\sum_{n=1}^{N}\frac{\Theta_n}{\Lambda_n} \times (1-e^{-\Lambda_n t})\Psi_n(s)^2 - 4\bar{\chi}(r_0,t)t, \tag{14}$$

where D_1 and D_2 are the diffusion constants in the case of relative diffusion of two spherical particles, D_{par} is the diffusion constant of the free particle in the case of the polymer-particle reaction, D_{pol} is the polymer's center-of-mass diffusion constant, and the sums over the mode numbers n again characterize the polymer's contour fluctuations [compare Eq. (8)]. The slowing down of the relative motion due to hydrodynamics is reflected by the effective coupling parameter $\bar{\chi}(r_0,t)$, which is motivated and shown in its full functional form in Appendix C. The nonhydrodynamic and hydrodynamic Green's functions for the two systems we considered are compared with BD results in Sec. IV.

III. BROWNIAN DYNAMICS SIMULATIONS

To test the analytic results of Sec. II, we simulate a semi-flexible polymer in solution adopting a standard BD scheme,[32] in which the polymer is modeled as a chain of M beads of radius a. For the low Reynolds number regime, the Langevin equation governing the time evolution of the position r_i of bead i is given by

$$\frac{d\boldsymbol{r}_i(t)}{dt} = \sum_{j=1}^{M} \overset{\leftrightarrow}{\boldsymbol{\mu}}_{ij} \cdot \underbrace{\left(-\frac{\partial U(\boldsymbol{r}_1,\ldots,\boldsymbol{r}_M)}{\partial \boldsymbol{r}_j} \right)}_{f_j(t)} + \boldsymbol{\xi}_i(t). \qquad (15)$$

The long-range hydrodynamic interactions—the fact that a force $\boldsymbol{f}_j$ acting on bead j creates a flow-field affecting the motion of bead i—are described by the Rotne–Prager mobility matrix $\overset{\leftrightarrow}{\boldsymbol{\mu}}_{ij}$ (Ref. 33)

$$\overset{\leftrightarrow}{\boldsymbol{\mu}}_{ij} = \mu_0 \delta_{ij} \overset{\leftrightarrow}{\mathbf{1}} + (1-\delta_{ij}) \overset{\leftrightarrow}{\boldsymbol{\mu}}(\boldsymbol{r}_{ij}), \qquad (16)$$

$$\overset{\leftrightarrow}{\boldsymbol{\mu}}(\boldsymbol{r}_{ij}) = \frac{1}{8\pi\eta r_{ij}}\left[\overset{\leftrightarrow}{\mathbf{1}} + \frac{\boldsymbol{r}_{ij}\otimes\boldsymbol{r}_{ij}}{r_{ij}^2} \right] + \frac{a^2}{4\pi\eta r_{ij}^3}\left[\frac{\overset{\leftrightarrow}{\mathbf{1}}}{3} - \frac{\boldsymbol{r}_{ij}\otimes\boldsymbol{r}_{ij}}{r_{ij}^2} \right], \qquad (17)$$

where $\boldsymbol{r}_{ij}=\boldsymbol{r}_i-\boldsymbol{r}_j$, $r_{ij}=|\boldsymbol{r}_{ij}|$, $\overset{\leftrightarrow}{\mathbf{1}}$ is the 3×3 identity matrix, and $\mu_0=(6\pi\eta a)^{-1}$ is the Stokes self-mobility of a sphere of radius a in a solvent of viscosity η. The stochastic contributions $\boldsymbol{\xi}_i(t)$ in Eq. (15) are assumed to be Gaussian random vectors, which are hydrodynamically correlated according to the fluctuation-dissipation theorem

$$\langle \boldsymbol{\xi}_i(t) \otimes \boldsymbol{\xi}_j(t') \rangle = 2k_B T \overset{\leftrightarrow}{\boldsymbol{\mu}}_{ij} \delta(t-t'). \qquad (18)$$

The interbead potential $U=U_{\text{WLC}}+U_{\text{LJ}}$ determining the configuration-dependent forces, where

$$U_{\text{WLC}} = \frac{\gamma}{4a}\sum_{i=1}^{M-1}(r_{i+1,i}-2a)^2 + \frac{\kappa}{2a}\sum_{i=2}^{M-1}(1-\cos\theta_i),$$

$$U_{\text{LJ}} = w\sum_{i<j}\Theta(2a-r_{ij})\left[\left(\frac{2a}{r_{ij}}\right)^{12} - 2\left(\frac{2a}{r_{ij}}\right)^6 + 1\right], \qquad (19)$$

consists of a shifted harmonic potential between adjacent beads of strength $\gamma=200k_B T/a$, a bending potential of strength $\kappa=l_p k_B T$ between adjacent bonds, and a pairwise truncated Lennard-Jones potential U_{LJ} of strength $w=3k_B T$. Here θ_i is the angle between the bond vectors $\boldsymbol{r}_{i,i-1}$ and $\boldsymbol{r}_{i+1,i}$. The first term in the wormlike chain potential U_{WLC} keeps the contour length L approximately fixed, while the second one with modulus κ takes care of the bending stiffness of the chain. The repulsive Lennard-Jones potential U_{LJ} prevents significant bead overlap, which is a source of numerical instabilities. In Sec. IV, where we model the motion of a free particle (i.e., a protein or free monomer) relative to the polymer chain, the particle is represented by an additional bead, not connected to the polymer chain, and subject only to hydrodynamic interactions between the particle and the chain. We do not account for steric interactions between particle and polymer in order to simplify the comparison with the theoretical results where such effects cannot be properly in-

cluded. A short discussion of excluded-volume effects is given in Appendix A. To avoid numerical instabilities in situations where the free particle overlaps with the polymer, in this case we use the Rotne–Prager–Yamakawa tensor,[34] which modifies Eq. (17) for overlapping beads to

$$\overset{\leftrightarrow}{\boldsymbol{\mu}}(\boldsymbol{r}_{ij}) = \mu_0\left[\left(1 - \frac{9r_{ij}}{32a}\right)\overset{\leftrightarrow}{\mathbf{1}} + \frac{3r_{ij}}{32a}\frac{\boldsymbol{r}_{ij}\otimes\boldsymbol{r}_{ij}}{r_{ij}^2}\right] \quad \text{if } r_{ij}\leq 2a. \qquad (20)$$

Equation (15) is discretized and integrated numerically using the Euler algorithm. The correlated stochastic contributions of Eq. (18) are obtained from uncorrelated Gaussian noise by means of a Cholesky decomposition of the hydrodynamic matrix $\overset{\leftrightarrow}{\boldsymbol{\mu}}_{ij}$. In all the results below, lengths are measured in units of a, energies in units of $k_B T$ and time in units of $\tau=a^2/(k_B T\mu_0)$. The time step is $\Delta t=3\times10^{-4}\tau$ and a typical simulation lasts 10^9 steps, after an initial thermalization period of 10^6–10^7 steps. To reduce computational costs the Cholesky decomposition is only performed every 5 time steps. For a given chain length $L=2a(M-1)$ and persistence length l_p, the quantities of interest are averaged over 25–2500 different trajectories until the convergence is satisfactory.

IV. RESULTS

In order to validate the various analytical approaches described in Sec. II, we test them against BD simulations. Since the binding rates depend sensitively on having good estimates for the Green's functions, we will focus on showing that the MFT approximation for the transition probabilities can reproduce the crucial physical effects: (i) the influence of internal polymer modes on the diffusion of the target site; (ii) the slow-down of relative motion between the free particle and target due to hydrodynamics. For simplicity, we concentrate in our analysis on one particular target site, the end-monomer of the chain. This has special relevance in biological processes, for example in the case of polymerization. Nevertheless, our theoretical approach is equally applicable to other target positions along the polymer contour: the results are similar though changes in the association rates are clearly less drastic because of the reduced mobility of target sites in the middle of the chain compared with the one at the chain's end.

A. Polymer motion

We begin by considering just the internal relaxation of a polymer of total contour length L: the radial Green's function of Eqs. (8) and (9) describing the diffusive motion of the polymer end-point ($s=\pm L/2$). In Fig. 1, we compare this analytical MFT expression for $G_{\text{rad}}(r,t)$ to histograms extracted from simulations of a chain with $L=100a$, $l_p=20a$. The histograms are based on the analysis of 25 independent trajectories, each with 10^8 steps. The time evolution of the probability distribution is in excellent agreement with $G_{\text{rad}}(r,t)$ [Eqs. (8) and (9)] over time scales spanning four orders of magnitude. Note that the largest time scale considered ($t=300\tau$) is less than the largest relaxation time of the
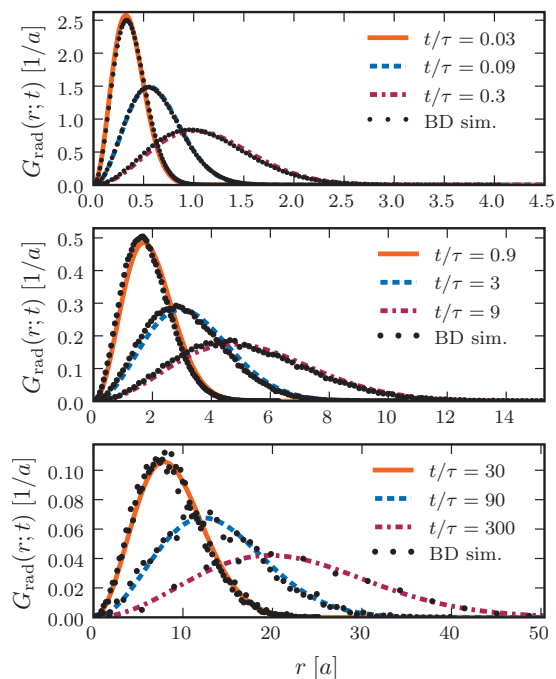
FIG. 1. The probability $G_{rad}(r,t)$ that the end-point of a polymer with length $L=100a$ and persistence length $l_p=20a$ will diffuse a distance r in time t. The MFT predictions [Eqs. (8) and (9), lines] are compared with the results from hydrodynamic BD simulations (black dots) for different times t measured in units of $\tau=a^2/(k_B T \mu_0)$.

polymer, $\Lambda_1^{-1} \sim 2 \times 10^3 \tau$, meaning that internal fluctuations dominate the polymer motion throughout this entire time range; the time evolution is illustrated more directly in the movie linked in Fig. 2 showing the remarkable agreement, even in the tails of the distribution (which are visible on the logarithmic scale spanning seven decades of magnitude). Our comparison here is more detailed than in the earlier MFT study of Ref. 29, since we consider the full transition probability and not just the end-point MSD. However, the conclusion is the same: the MFT provides a highly accurate picture of internal polymer dynamics.
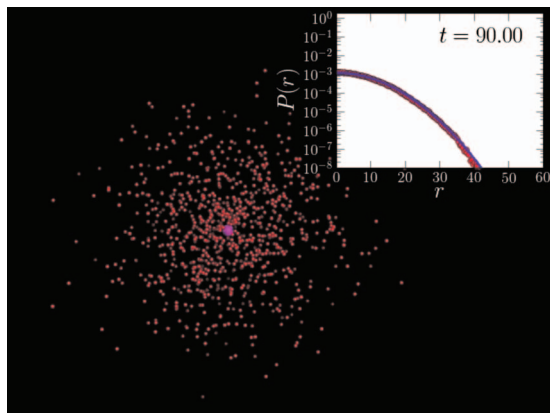

FIG. 2. The movie shows the motion of polymer end-points (red dots) superimposed from an ensemble of simulation trajectories, each starting at the origin (purple dot). The inset shows the evolving radial probability $P(r,t)=G_{rad}(r;t)/r^2$ taken from the simulation histograms (red markers) compared with the analytic MFT results of Eqs. (8) and (9) (blue curve). (Enhanced online.) [URL: http://dx.doi.org/10.1063/1.3352571.1]
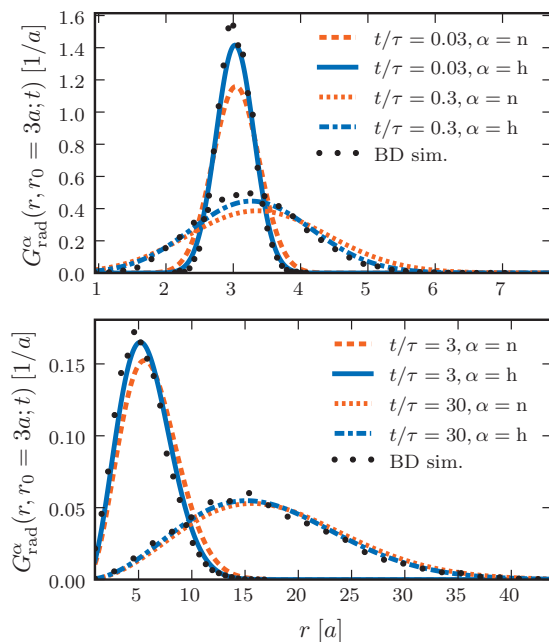

FIG. 3. The probability $G_{rad}^{\alpha}(r,r_0;t)$ that two spherical particles of radius a end up at separation r after time t given an initial separation $r_0=3a$. For each time t, BD simulation data including hydrodynamics (black dots) are compared with two theoretical results: the nonhydrodynamic Green's function for decoupled particles labeled by $\alpha=n$ [Eqs. (10) and (11)] and the approximate hydrodynamic Green's function labeled by $\alpha=h$ [Eqs. (10) and (12)]. Times are measured in units of $\tau=a^2/(k_B T \mu_0)$.

B. Relative motion of two spherical particles including hydrodynamics

Since the heuristic estimate for the hydrodynamic Green's function $G_{rad}^h(r,r_0;t)$ of two freely diffusing particles [Eqs. (10) and (12)] is the basis of our approach to polymer-particle interactions, we need to check that this estimate is reasonable. For this purpose, we performed hydrodynamic BD simulations of two single spheres of radius a and extracted histograms from the variation of the interbead distance over time. In total 2400 independent trajectories were calculated, each starting at a distance $r_{init}=3a$ and lasting 10^7 time steps. For given separations r_0 and r, relevant transition events were identified, i.e., parts of the trajectories starting at a certain distance $r_0 \pm \delta r/2$ and ending at $r \pm \delta r/2$, where δr is the histogram binwidth. These were used to estimate the probability distribution corresponding to $G_{rad}^h(r,r_0;t)$. In Fig. 3, we show the BD simulation results for $r_0=3a$ and various t together with G_{rad}^h [Eqs. (10) and (12)] and the hydrodynamically decoupled Green's function G_{rad}^n [Eqs. (10) and (11)]. Analogous results for an initial separation $r_0=5a$ are shown in Fig. 4. The inhibition of relative motion due to hydrodynamics is clearly evident at short times: the distributions from the simulations are more narrowly peaked than the decoupled results, which spread out noticeably faster. The slowing down is correctly reproduced in the G_{rad}^h curves, though it is slightly underestimated when compared with the simulation data. Despite the simplicity of the underlying approximation, G_{rad}^h still captures the essential features of the interaction. For longer times, when the interparticle distance has become large and hydrodynamics plays a smaller role, G_{rad}^h converges to G_{rad}^n, and both agree with the BD results.
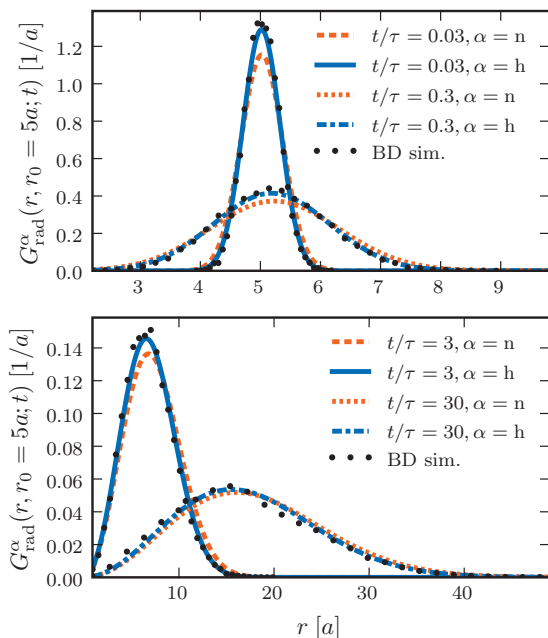
FIG. 4. Same as in Fig. 3, but with initial separation $r_0=5a$ between the beads.

C. Relative motion of a polymer and a spherical particle including hydrodynamics

The final test for our Green's function approach concerns the approximate description of polymer-particle relative motion, contained in Eqs. (10) and (14). To extract the corresponding transition probabilities from BD simulations, we take a polymer with $L=100a$, $l_\mathrm{p}=20a$, allow it to thermalize, and then add a single free particle of radius a that has no excluded volume, but is hydrodynamically coupled to the polymer beads. The particle is positioned at an initial distance $r_\mathrm{init}=3a$ from one of the polymer ends, and data is collected over 10^7 time steps. This procedure is repeated to obtain 2500 independent trajectories. As before, relevant transition events are used to determine the probability distribution for diffusing from a separation r_0 to r in time t. The results, plotted in Fig. 5 for $r_0=3a$ and in Fig. 6 for $r_0=5a$, are qualitatively similar to the case of two particles: compared with the nonhydrodynamic case we see a reduced relative mobility between the target site and the particle for small separations. The hydrodynamic Green's function is quite close to the simulation results, again slightly underestimating the strength of the coupling. However, given the complexity of the correlations between the particle and the entire polymer coil, it is notable that we are able to get good quantitative agreement. Since the association rates are derived directly from this Green's function, we conclude that we should be able to obtain realistic estimates for the reaction process.

D. Association rates

The diffusion-limited reaction we consider is schematically illustrated in Fig. 7: free particles are absorbed by the reactive end-monomer of a chain as soon as the separation r reaches the absorption radius $r_\mathrm{a}=r_\mathrm{par}+a$. The association rate is calculated from the renewal approach in Sec. II, with the
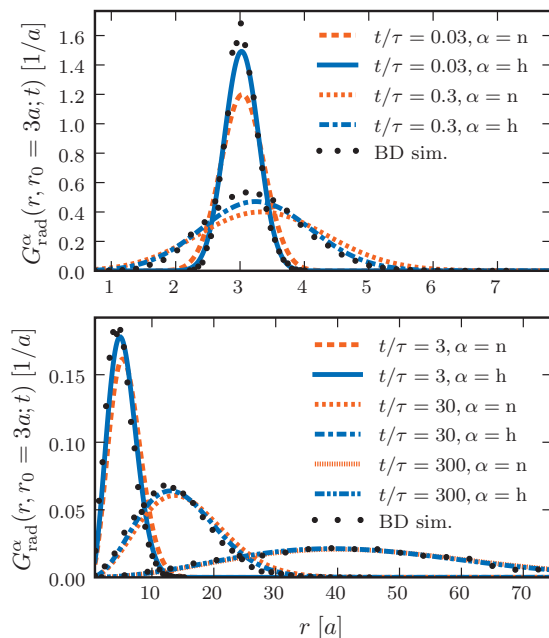

FIG. 5. The probability $G^\alpha_\mathrm{rad}(r,r_0;t)$ that the end-monomer of a polymer with $L=100a$, $l_\mathrm{p}=20a$, and a spherical particle of radius a end up at separation r after time t given an initial separation $r_0=3a$. For each time t, BD simulation data including hydrodynamics (black dots) are compared with two theoretical results: the nonhydrodynamic Green's function labeled by $\alpha=$n [Eqs. (10) and (13)], and the approximate hydrodynamic Green's function labeled by $\alpha=$h [Eqs. (10) and (14)]. Times are measured in units of $\tau=a^2/(k_\mathrm{B}T\mu_0)$.

only input being the radial Green's functions for the relative motion of the particle and the chain end [Eqs. (10) and (14)].

Since polymer fluctuations and the polymer-particle hydrodynamic coupling have competing effects on the association rate, it will be instructive to start with the simple case where the hydrodynamic coupling has been turned off, i.e., we use the nonhydrodynamic Green's function $G^\mathrm{n}_\mathrm{rad}$ of Eqs.
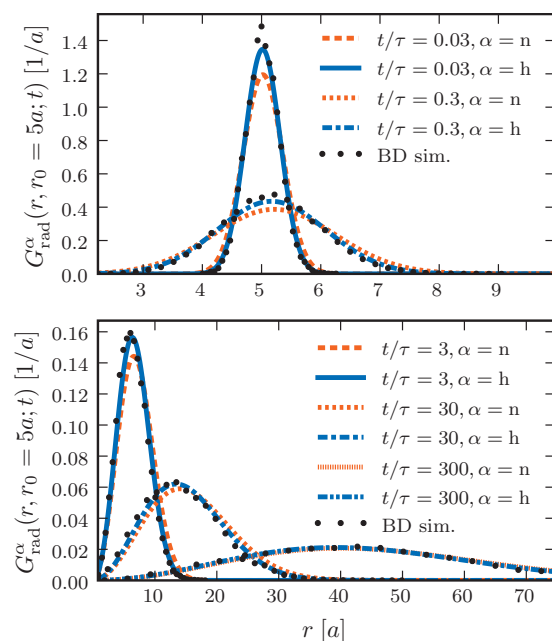

FIG. 6. Same as in Fig. 5, but with initial separation $r_0=5a$ between the end-monomer and the free particle.
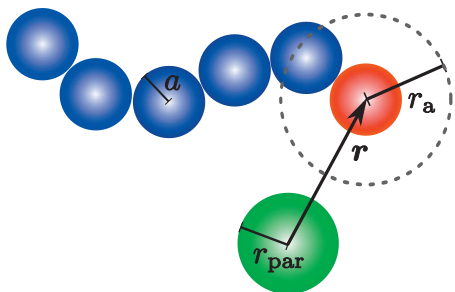
FIG. 7. Schematic view of a bead-spring polymer with a reactive end and a free particle of radius r_{par}. The particle is absorbed as soon as the separation r reaches the absorption radius $r_a = r_{par} + a$.

(10) and (13). The resulting association rate as a function of particle radius r_{par} for a polymer with $L = 1000a$, $l_p = 50a$ is marked by red dots in Fig. 8. (For DNA, where $a \approx 1$ nm and $l_p \approx 50$ nm, this would correspond to a strand of length 1 μm.) The Smoluchowski rate,

$$k_S = 4\pi(D_{pol} + D_{par})r_a, \qquad (21)$$

which involves only the center-of-mass motion of the polymer coil and particle, is shown as a line with the polymer diffusion constant D_{pol} taken from the MFT expansion in Appendix B. The corresponding numerical results of the renewal approach shown as green triangles are based on Eqs. (10) and (11) and again use D_{pol} from Appendix B. The Smoluchowski value is the standard point of reference when considering DNA-protein interaction.[35] Clearly, internal polymer fluctuations have a significant impact, enhancing the association rates by 50%–135% relative to k_S over the range $r_{par} = 0.5a - 6a$; the minimum at $r_{par} \approx 2a$ for the rates with internal polymer motion indicates that the effect of larger absorption radius $r_a = r_{par} + a$ with increasing r_{par} quickly
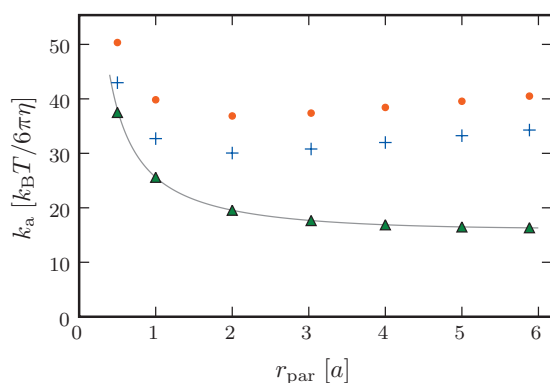

FIG. 8. Three estimates for the association rate of a free particle to the end-point of a polymer with $L = 1000a$, $l_p = 50a$, as a function of particle radius r_{par}. For DNA, where $a \approx 1$ nm and $l_p \approx 50$ nm, the corresponding strand would have a length $L = 1$ μm. The rates are measured in units of $k_B T / 6\pi\eta$, or $\approx 1.3 \times 10^8$ M^{-1} s^{-1} for water at room temperature. Green triangles and solid line are the Smoluchowski rate considering only the center-of-mass diffusion of the particle and the polymer coil, without hydrodynamic coupling [green triangles are based on Eqs. (10) and (11), the line denotes Eq. (21)]. Red dots: the rates including the internal fluctuations of the polymer, without hydrodynamics [Eqs. (10) and (13)]. Blue crosses: the total rates including both fluctuations and hydrodynamics [Eqs. (10) and (14)]. All the data marked by symbols is obtained from the numerical evaluation of the renewal approach [Eqs. (2)–(4)].

dominates the one of decreasing diffusion constant $D_{par} \propto r_{par}^{-1}$.

In the absence of hydrodynamics, we can use an earlier result of Berg[21] to do a consistency check on the renewal approach derivation of the association rates. For the case of a Gaussian Green's function, and assuming a Gaussian sink profile $S(r) = \exp(-3r^2/2r_a^2)$ instead of a perfectly absorbing boundary at r_a, Berg derived an expression for the association rate in terms of the relative nonhydrodynamic variance $V^n(t)$

$$k_a^{Berg} = (2\pi)^{3/2}\left[\int_0^\infty dt(V^n(t) + 2/3 r_a^2)^{-3/2}\right]^{-1}. \qquad (22)$$

Plugging $V^n(t)$ from Eq. (13) into Eq. (22), we recover the nonhydrodynamic rates shown in Fig. 8 within a difference of 5% (comparison not shown).

When hydrodynamic interactions are included together with internal polymer motion [G_{rad}^h of Eqs. (10) and (14) is used instead of G_{rad}^n of Eqs. (10) and (13)], the association rates are smaller than in the nonhydrodynamic case, as seen in the data marked by blue crosses in Fig. 8. This is due to the inhibited mobility between the particle and the target at short distances. However the rate decrease is only $\sim 15\% - 20\%$, so the overall association rate is still 30%–100% larger than the Smoluchowski result for the range of particle sizes considered. The magnitude of the rate decrease is comparable to previous estimates derived for the simpler problem of a reaction between two spherical particles: Friedman obtained a 15% reduction due to hydrodynamics,[36] Deutch and Felderhof saw a 46% drop-off,[37] and Wolynes and Deutch predicted a decrease by 29%.[38]

Since the conformational fluctuations depend on the mechanical properties of the chain, it is natural that the association rates will vary with the parameters L and l_p that characterize the semiflexible polymer. In Fig. 9, we show contour diagrams of the association rate in terms of L/a and l_p/a for two different particle radii: $r_{par} = a$ in the top panel, as would be the case in a polymerization process, and $r_{par} = 4a$ in the bottom panel, which corresponds to an average protein size for the case of DNA-protein interaction (with $a = 1$ nm). Figure 10 depicts the same data, but in terms of percent rate increase over the Smoluchowski result k_S of Eq. (21). Interestingly, while the absolute rate in Fig. 9 is almost independent of L for $L \gg l_p$, it does show a slight maximum for $l_p \approx 20a$ when $r_{par} = a$ and $l_p \approx 30a$ when $r_{par} = 4a$. This behavior as a function of l_p is an intrinsic property of the polymer, because it appears also in the absence of hydrodynamic coupling (data not shown). This means that there is an optimal persistence length l_p at which the chain reactivity is maximized, and interestingly this optimum is not far from the actual DNA persistence length of $l_p = 50$ nm. The maximum is more prominent in the relative rates of Fig. 10, where the increase compared with k_S rises sharply to $\sim 30\%$ ($r_{par} = a$) and $\sim 100\%$($r_{par} = 4a$) for long polymers with $l_p = 20a - 60a$ including double-stranded DNA ($l_p \approx 50a$).
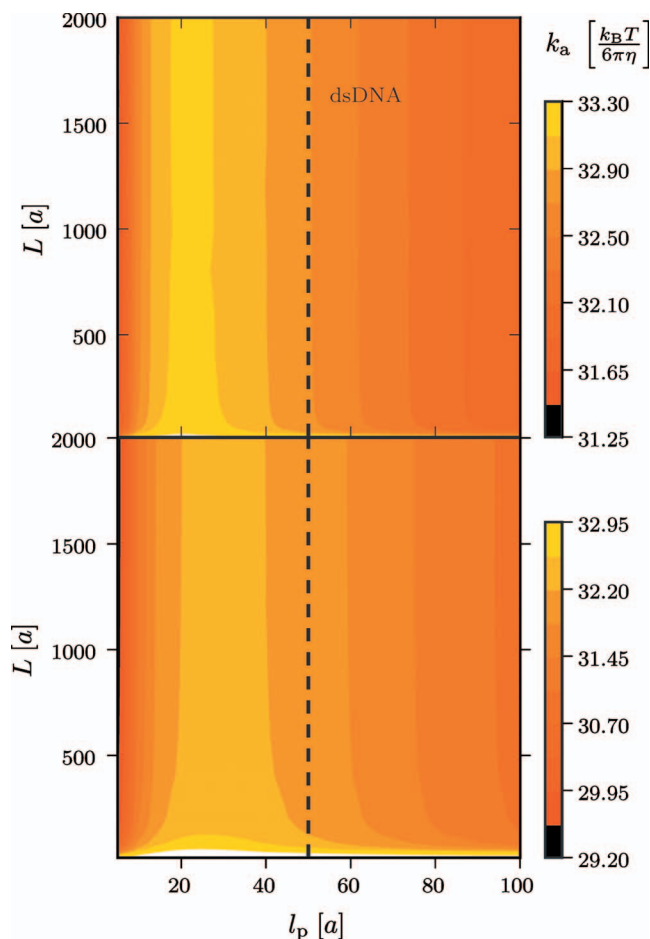
FIG. 9. The association rate k_a [Eqs. (2)–(4) with Eqs. (10) and (14)] between a free particle and a polymer end as it varies with the polymer contour length L and persistence length l_p for particle radius $r_{par} = a$ (top panel) and for $r_{par} = 4a$ (bottom panel). The rates include the effects of polymer fluctuations and hydrodynamic coupling, and are measured in units of $k_B T / 6\pi\eta$, or $\approx 1.3 \times 10^8$ M^{-1} s^{-1} in water at room temperature.

FIG. 10. Same as in Fig. 9, but showing the percent rate increase over the Smoluchowski result, k_S [Eq. (21)], instead of the absolute rate.

V. DISCUSSION AND SUMMARY

In this paper, we have studied the association of free particles and a target site on a semiflexible polymer—a class of diffusion-limited reactions of wide biological relevance, whether in polymerization of biomolecules or gene regulation by DNA-binding proteins. We focused on two competing effects that are, with the lone exception of the segmental diffusion considered in Ref. 21, entirely neglected in existing theories for these processes: the bending fluctuations of the polymer in equilibrium, which enhance the association rate, and the hydrodynamics between the polymer and particle, which reduces it. Quantifying the fluctuations required an accurate description of internal polymer motion, available through the MFT of semiflexible polymer dynamics. For the hydrodynamics, we developed a simple heuristic estimate to model the decrease in mobility when two diffusing objects approach each other. The end result of the competition sensitively depends on the mechanical properties of the polymer and the size of the reactive particle: we see a maximal increase over the Smoluchowski rate for persistence lengths $l_p = 20a - 60a$; this increase is ~30% for the case of small particles, and ~100% for particle sizes typical of regulatory proteins. As a function of particle size, the reaction rate dis-
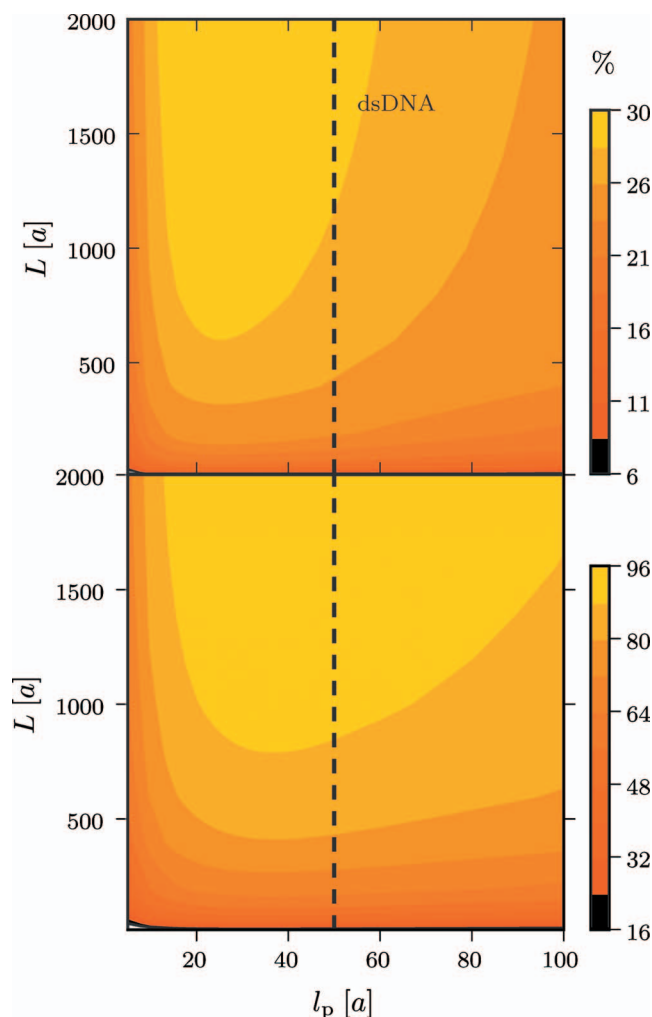
plays a minimum at a particle radius equal to the polymer diameter; for larger proteins the probability of hitting the DNA increases.

Although based on experimental evidence it is generally assumed that the binding of proteins to DNA is a diffusion-limited process[2] (and references therein), recent studies in the slightly different context of protein assisted interior loop formation of DNA[39,40] indicate that this assumption is probably not justified for all kinds of DNA-protein systems. Within our approach we have neglected the possibility of encounters between the protein and the target site on the DNA that do not immediately lead to a reaction, for example due to orientational constraints. This is clearly an oversimplification, which however can be approximately rectified by a reaction factor Γ (see Appendix A).

Directly testing our theoretical predictions may be possible with existing experimental techniques. In particular, one can study the role of polymer fluctuations on association rates by comparing two different setups involving bimolecular diffusion-limited reactions, shown schematically in Fig. 11. In scenario I both reactants are free in solution, while in scenario II one of the reactants is bound to the end of a semiflexible polymer. The corresponding rates k_a^I and k_a^{II} could be measured through simple kinetic experiments or
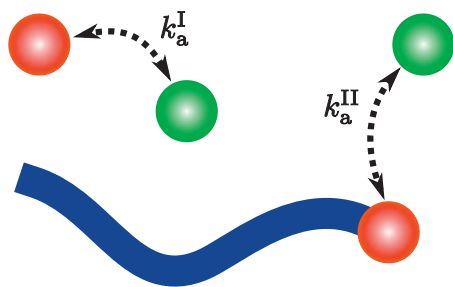
FIG. 11. Schematic representation of two scenarios for a bimolecular reaction: (I) both species are free in solution; (II) one of the species is attached to the end of a semiflexible polymer. The comparison of the diffusion-limited association rates k_a^I and k_a^{II} should highlight the role of internal polymer motion in such reactions.

using fluorescence microscopy. In the latter case, the reactants would be fluorophores and quencher molecules, and the rate of the diffusion-limited quenching reaction can be extracted from the decay of the total fluorescence signal over time. As shown in Table I, our theory predicts a ratio $k_a^{II}/k_a^I \approx 0.77$ for the two scenarios using $r_{par}=a$ and a 1 μm strand of DNA. This is clearly distinguishable from the Smoluchowski prediction, $k_a^{II}/k_a^I=0.5$, which ignores hydrodynamics and internal fluctuations.

ACKNOWLEDGMENTS

APPENDIX A: ADDITIONAL EFFECTS ON THE ASSOCIATION RATES

Throughout this paper we have considered an idealized picture of the association process assuming that a reaction takes place as soon as the radial distance r reaches the absorption radius r_a. A more realistic description should take into account a number of other factors: (i) molecules are in general not equally reactive on their entire surface, i.e., binding also depends on the relative orientation of the reactants; (ii) the correct relative orientation alone might not directly lead to binding due to additional requirements, e.g., conformational changes of the molecules. In addition we have assumed that the polymer-particle dynamics is purely diffusive; deviations from this behavior might be caused by (iii) excluded-volume effects between the particle and nontarget monomers of the polymer together with (iv) electrostatic interactions between the particle and polymer. Due to all these effects, the real rate $k_a^{real}=\Gamma k_a$ will differ from our predicted

TABLE I. Estimates for diffusion-controlled bimolecular association rates in the experimental scenarios shown in Fig. 11. The polymer is assumed to be a 1 μm strand of dsDNA and the particle radius $r_{par}=1$ nm. The rates k_a are given in units of $k_B T/6\pi\eta$ or $\approx 1.3\times10^8$ M^{-1} s^{-1} in water at room temperature.

Rate estimates including	k_a^I	k_a^{II}	k_a^{II}/k_a^I
Center-of-mass motion	50.27	25.14	0.5
Plus internal polymer motion	$\cdots$	39.83	$\cdots$
Plus hydrodynamics	42.52	32.71	0.77

rate k_a by a factor Γ. Below we give a rough estimate of Γ for each of these cases and argue that, though modifying the absolute values of the association rates, these considerations do not alter the main qualitative conclusions of our work.

(i) Rate-influencing effects of orientational constraints have been examined for the case of diffusion-controlled bimolecular reactions of spherical particles;[41,42] the general ideas can also be applied to our polymer-particle system. If only a fraction p of the target's surface is reactive, the most important result is that the association rate is *not* simply reduced by p. Rather the factor $\Gamma > p$ reflects the fact that a first encounter between the reactants involving inert parts of the target's surface (occurring with probability $1-p$) does not exclude the possibility of a successful reaction at a later time. In the limit where the process of mutual reorientation is fast compared with the time scale of relative diffusion, one even recovers $\Gamma=1$: the partial surface reactivity is then completely compensated for by fast orientational changes of the target. End-tangent fluctuations of semiflexible polymers are typically fast—the relaxation times of the high frequency normal modes are on the order of $\sim a^2/(\mu_0 k_B T) \approx 4$ ns. Plugging this time scale into the method of Ref. 42, one can extract representative values for Γ: when $p=0.5$ we find $\Gamma \approx 0.79$ for $r_{par}=a$ and $\Gamma \approx 0.91$ for $r_{par}=5a$.

(ii) For the case where the reaction is limited by the conformational state of the particle, the time scale of conformational transitions is typically much larger than the time scale of relative diffusion between the particle and the target. Where such a separation of time scales exists, the rate reduction factor Γ is approximately just the probability for the particle to be in the correct conformation.

(iii) Throughout this paper excluded-volume effects between polymer and particle have been neglected. The diffusion toward the target is altered by the presence of the polymer coil; however, since the effective segment density is low for a semiflexible polymer in good solvent, we only expect minor corrections. On the other hand, as can be seen from Fig. 7, neighboring monomers to the target monomer exclude a solid angle Ω^{ex} from the target's surface. In the case of the end-monomer being the target, the excluded solid angle is simply

$$\Omega^{ex} = \int_0^{2\pi} d\phi \int_0^{\theta^{max}} d\theta \sin\theta = 2\pi \frac{r_{par}}{r_{par}+a}, \quad (A1)$$

with $\theta^{max}=\arccos(r_{par}/(r_{par}+a))$. The surface of the target-monomer over which a reaction can take place is therefore reduced by a factor $p=1-\Omega^{ex}/4\pi$ ranging from 1 in the limit $r_{par}\to 0$ to 1/2 in the limit $r_{par} \to \infty$. At first glance the situation may appear similar to case (i), where a fraction $1-p$ of the target surface is inert. However here the $1-p$ fraction is inaccessible due to excluded volume; since the particle cannot get near to that portion of the target, the rate reduction

will be less drastic (for a given p, the corresponding Γ value will be closer to 1).

(iv)   For electrostatic effects, which play a role, for example, in the nonspecific interactions between proteins and DNA, the value of Γ is difficult to estimate analytically. An effective method for determining Γ using BD simulations has been proposed in Ref. 43; the authors of that study considered attractive electrostatics between oppositely charged monovalent ions in water. For an unscreened Coulomb potential Γ = 6.82 and 7.31, respectively, with and without hydrodynamic interactions on the level of the Oseen tensor. The corresponding values for a Debye length of 1 nm were Γ = 4.40 and 4.80.

The total value of Γ seen in an experimental situation is expected to reflect some combination of the above effects. While this will modify the absolute association rates, the relative rate changes discussed in our work should remain valid: in all scenarios, when we compare to a fixed target in the free-draining limit, the inclusion of hydrodynamics should retard the reaction, but should be more than compensated for by the speed-up due to internal polymer fluctuations.

APPENDIX B: MEAN FIELD THEORY FOR SEMIFLEXIBLE POLYMER DYNAMICS

The simplest description of a semiflexible polymer is the wormlike chain model: the polymer is represented by a continuous, differentiable space curve $r(s)$ of contour length L, where the arc-length variable s ranges from $-L/2$ to $L/2$. The associated elastic energy U_{WLC}, the continuum analog of Eq. (19), is given by[44]

$$U_{\mathrm{WLC}}[r(s)] = \frac{\kappa}{2} \int_{-L/2}^{L/2} ds \left(\frac{\partial u(s)}{\partial s} \right)^2. \tag{B1}$$

The bending rigidity is $\kappa = l_p k_B T$, and the tangent vector $u = \partial r / \partial s$ is constrained by local inextensibility to unit length, $u^2(s) = 1$ at each s. Since this constraint leads to nonlinear equations of motion, an alternative, approximate model is required. Within the MFT approach[45,46] the local constraint is relaxed and replaced by the global and end-point conditions $\langle \int ds u^2(s) \rangle = L$ and $\langle u^2(\pm L/2) \rangle = 1$. The result is a Gaussian mean field Hamiltonian which incorporates a finite extensibility in addition to the bending term

$$U_{\mathrm{MF}}[r(s)] = \frac{\epsilon}{2} \int_{-L/2}^{L/2} ds \left(\frac{\partial u(s)}{\partial s} \right)^2 + \nu \int_{-L/2}^{L/2} ds u^2(s)$$
$$+ \nu_0 (u^2(L/2) + u^2(-L/2)), \tag{B2}$$

where $\epsilon = 3 l_p k_B T / 2$, $\nu = 3 k_B T / (4 l_p)$, and $\nu_0 = 3 k_B T / 4$. In this form the Gaussian model exactly reproduces various lowest-order equilibrium averages of the wormlike chain, most importantly the tangent-tangent correlation function, and other derived quantities such as the mean square end-to-end distance.

The dynamic theory for the Gaussian semiflexible polymer is based on the hydrodynamic preaveraging approach of

Ref. 47, analogous to that used for the Zimm model[48] in the case of flexible chains. The time evolution of a point s on the polymer contour is governed by the Langevin equation

$$\frac{\partial}{\partial s} r(s,t) = -\int_{-L/2}^{L/2} ds' \, \vec{\vec{\mu}}_{\mathrm{av}}(s,s') \frac{\delta U_{\mathrm{MF}}}{\delta r(s',t)} + \xi(s,t),$$
$$\tag{B3}$$
$$\langle \xi(s,t) \otimes \xi(s',t') \rangle = 2 k_B T \vec{\vec{\mu}}_{\mathrm{av}}(s,s') \delta(t-t').$$

Here we use the preaveraged mobility tensor $\vec{\vec{\mu}}_{\mathrm{av}}(s,s')$, which is obtained from the standard Rotne–Prager tensor by averaging over all equilibrium configurations of the polymer. As seen in Eq. (17), the original Rotne–Prager mobility involves a dependence on the spatial distance between polymer points, and hence on the specific configuration of the chain. This would lead to nonlinear equations of motion, a problem which is resolved in the preaveraging approximation, where the mobility depends only on the arc-length coordinates s and s'. For the mean field model of Eq. (B1) the preaveraged mobility has the form[47]

$$\vec{\vec{\mu}}_{\mathrm{av}}(s,s') = \left[2 a \mu_0 \delta(s-s') + \frac{\Theta(|s-s'|-2a)}{\eta \sqrt{6 \pi^3 \sigma(|s-s'|)}} \right.$$
$$\left. \times \exp\left(-\frac{6a^2}{\sigma(|s-s'|)} \right) \right] \vec{\vec{1}}, \tag{B4}$$

where $\sigma(l) = 2 l_p l - 2 l_p^2 (1 - \exp(-l/l_p))$. The microscopic length scale a in the continuum theory corresponds to the monomer radius in the discrete BD simulations, and the unit step function Θ in Eq. (B4) serves as a short-distance cutoff for the hydrodynamic interactions.

The preaveraged Langevin equation can be solved through a normal mode decomposition, with the eigenmodes fulfilling free-end boundary conditions at $s = \pm L/2$. This reduces Eq. (B3) to a set of ordinary differential equations coupled by a hydrodynamic interaction matrix; the diagonalization of this matrix yields simple Langevin equations for the decoupled normal mode amplitudes $P_n(t)$ [with stochastic contributions $Q_n(t)$]

$$\frac{\partial}{\partial t} P_0(t) = \mathbf{Q}_0(t), \quad \frac{\partial}{\partial t} P_n(t) = -\Lambda_n P_n(t) + \mathbf{Q}_n(t),$$

$$n = 1, \ldots, N, \tag{B5}$$

$$\langle Q_{ni}(t) Q_{mj}(t') \rangle = 2 k_B T \delta_{ij} \delta(t-t') \Theta_n \delta_{nm}.$$

The vectors $P_n(t)$ and $Q_n(t)$ are related to $r(s,t)$ and the stochastic velocities $\xi(s,t)$ through the expansions $r(s,t) = \Sigma_{n=0}^N P_n(t) \Psi_n(s)$ and $\xi(s,t) = \Sigma_{n=0}^N Q_n(t) \Psi_n(s)$, where the scalar functions $\Psi_n(s)$ are the decoupled normal modes. The modes are ordered in such a way that the eigenvalues Λ_n (inverse relaxation times) increase with n. Following Ref. 29, we set the high-frequency cutoff N for the mode number to $N = [L/8a]$, which was shown to give good agreement at short times with BD simulations. At longer times, where the polymer fluctuations are at length scales much larger than the monomer radius a, the dynamics does not depend on the precise choice of the cutoff. Λ_n and the fluctuation-dissipation parameters Θ_n can be directly derived from the

tensor $\vec{\tilde{\mu}}_{\mathrm{av}}$ evaluated numerically in the normal mode basis. Full details of this procedure, together with the explicit form of the normal modes $\Psi_n(s)$, are given in Ref. 29.

Equation (B5) for a given mode n can be mapped onto the well-known problem of a particle diffusing with friction constant ζ in a harmonic potential of strength k centered at $x=0$.[49] We identify the mode amplitude $P_n(t)$ with the position x of the particle and set $\Lambda_n = k/\zeta$, $\Theta_n = 1/\zeta$. This allows us to calculate the explicit form of the Green's function for the diffusive process, in other words the transition probability $P(P_n(t), P_n(0); t)$ for observing the amplitude $P_n(t)$ after time t, starting from the initial amplitude $P_n(0)$

$$P(P_n(t), P_n(0); t) = (2\pi\sigma_n^2(t))^{-3/2} \exp\left(-\frac{(P_n(t) - M_n(t))^2}{2\sigma_n^2(t)}\right).$$

$$\text{(B6)}$$

The probability has the form of a spreading Gaussian, with time-dependent mean $M_n(t)$ and variance $\sigma_n^2(t)$ given by

$$M_0(t) = P_0(0), \quad M_n(t) = P_n(0) e^{-\Lambda_n t}, \quad \forall \, n > 0, \quad \text{(B7)}$$

$$\sigma_0^2(t) = 2L D_{\mathrm{pol}} t, \quad \sigma_n^2(t) = k_B T \Theta_n \Lambda_n^{-1} (1 - e^{-2\Lambda_n t}), \quad \forall \, n > 0.$$

$$\text{(B8)}$$

Here

$$D_{\mathrm{pol}} \equiv k_B T \Theta_0 \Psi_0(s)^2 = k_B T \Theta_0 \frac{1}{L}, \quad \text{(B9)}$$

denotes the center-of-mass diffusion constant of the polymer coil. Modes with different mode number n evolve independently of each other. Transition probabilities between different polymer configurations, each of them corresponding to a certain (unique) set of normal mode amplitudes $\{P_n(t)\}$, are therefore expressed as the product of the transition probabilities for the individual modes. As we are interested in the motion of a single point s on the polymer contour, the integrations over initial configurations with $r(s,0) = r_0$ and final configurations with $r(s,t) = r$ can be readily performed yielding the Green's function in Eqs. (7) and (8).

APPENDIX C: HYDRODYNAMIC INTERACTIONS

In Appendix B, we were able to describe the long-range hydrodynamic interactions between various points on a polymer coil, and their influence on the internal relaxation of the chain. A key simplifying feature in this analysis is the fact that the spatial relationship between any two points on the contour is constrained: their hydrodynamic interactions as the polymer fluctuates in equilibrium can be taken into account through the preaveraging approximation. For the case of a free particle and a target site on the polymer coil, estimating hydrodynamic interactions is more difficult: the particle can drift away, and the strength of the interaction will be highly dependent on the initial conditions and the elapsed time. To understand the role of hydrodynamics in this situation, we first consider the simpler case of two freely diffusing spherical particles, before tackling the full problem of

polymer-particle hydrodynamics. Though it may seem trivial, even the two particle case presents a challenging problem.[36,37]

1. Case of two spherical particles

We consider two noninteracting particles at positions $r_i(t)$, $i = 1, 2$, described by the Langevin equations

$$\frac{\partial}{\partial t} r_i(t) = \xi_i(t),$$

$$\text{(C1)}$$

$$\langle \xi_i(t) \otimes \xi_j(t') \rangle = 2k_B T \delta(t - t')[\delta_{ij} \mu_i \vec{\mathbf{1}} + (1 - \delta_{ij}) \vec{\tilde{\mu}}(r_{12})],$$

where μ_i is the self-mobility of particle i, and hydrodynamics are expressed through the Rotne–Prager tensor $\vec{\tilde{\mu}}(r_{12})$, defined in Eq. (17), dependent on the interparticle separation r_{12}. Hydrodynamic interactions are long-ranged ($\propto r_{12}^{-1}$) and therefore negligible only at distances much larger than the sum of the particle radii, $r_{12} \gg a_1 + a_2$. For small separations, the stochastic motion of the particles is highly correlated, leading to a decrease in their relative mobility. To get a realistic estimate of binding rates, where particles clearly have to approach each other, it is therefore necessary to take these hydrodynamic effects into consideration.

The main quantity of interest is the radial Green's function for the relative motion of the particles, the probability that two particles starting from a distance $r_0 = |r_{12}(0)|$ reach a distance $r = |r_{12}(t)|$ in time t. For comparison, we will consider the situation both with and without hydrodynamic interactions, labeling the respective Green's function $G_{\mathrm{rad}}^{\mathrm{h}}$ and $G_{\mathrm{rad}}^{\mathrm{n}}$. The second case, where the particles are totally decoupled and only the self-mobilities enter into the stochastic correlations of Eq. (C1), is trivial and leads to the functional form of Eq. (10) with the variance of Eq. (11), where $D_i = \mu_i k_B T$ is the diffusion constant of particle i. Note that the variance $V^{\mathrm{n}}(t)$ is just 1/3 of the MSD $\langle (r_{12}(t) - r_{12}(0))^2 \rangle$.

In contrast, for the hydrodynamic case one cannot derive an analytical form for $G_{\mathrm{rad}}^{\mathrm{h}}$. Thus we will have to resort to a heuristic approximation: we assume $G_{\mathrm{rad}}^{\mathrm{h}}$ has the same functional form as Eq. (10), but with a different variance $V^{\mathrm{h}}(t)$, reflecting the slower relative motion of the particles. Since this variance is related to the MSD of $r_{12}(t)$, we begin by evaluating this MSD. From Eq. (C1) and the definition of the Rotne–Prager tensor, Eq. (17), one can obtain the following exact relationship:

$$\langle (r_{12}(t) - r_{12}(0))^2 \rangle$$

$$= 6(D_1 + D_2)t - 12k_B T \underbrace{\left\langle \int_0^t dt' \frac{1}{6\pi\eta r_{12}(t')} \right\rangle}_{\equiv \chi t}.$$

$$\text{(C2)}$$

The second term on the right can be rewritten as $-12\chi t$, defining a time-dependent coupling parameter χ, which quantifies the slow-down in relative diffusion compared with the nonhydrodynamic case. This parameter involves both a time and ensemble average over the trajectory $r_{12}(t)$, and hence is also dependent on the initial separation r_0. Our heuristic approach approximates χ by an effective coupling

function $\bar{\chi}(r_0,t)$, where the time and ensemble averages have been replaced by a single ensemble average involving the Green's function $G_{\mathrm{rad}}^{\mathrm{n}}$ for the nonhydrodynamic system

$$
\begin{aligned}
\bar{\chi}(r_0,t) &= \frac{k_{\mathrm{B}}T}{6\pi\eta} \int_{r_a}^{\infty} dr \frac{1}{r} G_{\mathrm{rad}}^{\mathrm{n}}(r,r_0;t) \\
&= \frac{k_{\mathrm{B}}T}{6\pi\eta} \frac{1}{2r_0} \left[\mathrm{erf}\left(\frac{r_0 - r_a}{\sqrt{2V^{\mathrm{n}}(t)}} \right) + \mathrm{erf}\left(\frac{r_0 + r_a}{\sqrt{2V^{\mathrm{n}(t)}}} \right) \right].
\end{aligned}
$$

(C3)

As in the preaveraging approximation in Appendix B, hydrodynamic interactions are cut off below the distance $r_a = a_1 + a_2$, where the particles overlap. This effective parameter shows the correct limiting behavior: $\bar{\chi}(r_0,t) \propto r_0^{-1}$ for short times, where particles are close to their initial separation, and $\bar{\chi}(r_0,t) \propto ((D_1+D_2)t)^{-1/2}$ for long times where the particles have drifted far away from each other. In analogy to the nonhydrodynamic case, we define the variance $V^{\mathrm{h}}(t)$ as 1/3 of the MSD, using the effective parameter $\bar{\chi}(r_0,t)$ instead of χ. Thus the final form for our approximate hydrodynamic Green's function is reflected in Eqs. (10) and (12). The role of the effective coupling parameter $\bar{\chi}$ is to reduce the relative mobility of the particles when they are near to each other and thus subject to strong hydrodynamic interactions; in the long-time limit the hydrodynamic effects become negligible as the particles move to large separations.

In principle, the procedure outlined above to estimate χ can be iterated to produce higher-order approximations: in deriving $\bar{\chi}(r_0,t)$ one can use the hydrodynamic Green's function $G_{\mathrm{rad}}^{\mathrm{h}}$ of Eqs. (10) and (12) instead of $G_{\mathrm{rad}}^{\mathrm{n}}$. This would lead to a better approximation for χ, and hence a more accurate Green's function which could be input into the next level of the approximation. This iterative method converges quickly, so for simplicity we restrict ourselves to the first order results.

2. Case of a DNA-target site and a free particle

This approach for two freely diffusing particles can be generalized to the problem of a free particle and a polymer. The nonhydrodynamic case is again simple, with the relative motion of the particle and a point s on the chain described by a radial Green's function which has exactly the same form as Eq. (10). The only difference is the variance $V^{\mathrm{n}}(t)$, which now includes the contribution of the polymer's internal modes as shown in Eq. (13). Here $D_{\mathrm{par}} = k_{\mathrm{B}}T/6\pi\eta r_{\mathrm{par}}$ is the diffusion constant of the free particle, and r_{par} is the particle radius.

For the hydrodynamic case, we can divide the complicated interactions between the particle and the chain into three parts: (i) the influence of the local region of radius a around the target site s on the free particle; (ii) the influence of the rest of the chain on the particle; and (iii) the back influence of the particle on the entire polymer. For the specific problem we consider—association rates to a given target site—hydrodynamics plays a significant role only in the close vicinity of the target. Hence contribution (i) will dominate. The back influence in (iii) should be negligible for free particles comparable in size to the monomers in the chain,

$r_{\mathrm{par}} \sim \mathcal{O}(a)$, since the motion of the polymer is mainly governed by relaxation of the internal modes. The relative unimportance of (ii) is more subtle: one can take it into account in a more elaborate numerical evaluation of the preaveraged MFT Langevin equations, but comparison with the simpler approximation discussed below does not show significant improvement with respect to BD simulations (which include all three contributions). Thus we can construct a simple estimate for the hydrodynamic Green's function by focusing on contribution (i). $G_{\mathrm{rad}}^{\mathrm{h}}$ has the same form as the two-particle case, Eq. (10), but with a variance given by Eq. (14) with

$$
\bar{\chi}(r_0,t) = \frac{k_{\mathrm{B}}T}{6\pi\eta} \frac{1}{2r_0} \left[\mathrm{erf}\left(\frac{r_0 - r_a}{\sqrt{2V^{\mathrm{n}}(t)}} \right) + \mathrm{erf}\left(\frac{r_0 + r_a}{\sqrt{2V^{\mathrm{n}(t)}}} \right) \right],
$$

(C4)

in analogy to Eq. (12). Here $V^{\mathrm{n}}(t)$ is the nonhydrodynamic polymer-particle variance of Eq. (13). In this way we have accounted for both the internal fluctuations of the target site and, through $\bar{\chi}(r_0,t)$, the decrease in relative mobility for the approaching particle.

[1] O. G. Berg and P. H. Vonhippel, Annu. Rev. Biophys. Biophys. Chem. **14**, 131 (1985).
[2] S. E. Halford and J. F. Marko, Nucleic Acids Res. **32**, 3040 (2004).
[3] R. F. Bruinsma, Physica A **313**, 211 (2002).
[4] A. D. Riggs, W. Bourgeois, and M. Cohn, J. Mol. Biol. **53**, 401 (1970).
[5] O. G. Berg, R. B. Winter, and P. H. von Hippel, Biochemistry **20**, 6929 (1981).
[6] R. B. Winter and P. H. von Hippel, Biochemistry **20**, 6948 (1981).
[7] R. B. Winter, O. G. Berg, and P. H. von Hippel, Biochemistry **20**, 6961 (1981).
[8] Y. M. Wang, R. H. Austin, and E. C. Cox, Phys. Rev. Lett. **97**, 048302 (2006).
[9] I. Bonnet, A. Biebricher, P. L. Porte, C. Loverdo, O. Benichou, R. Voituriez, C. Escude, W. Wende, A. Pingoud, and P. Desbiolles, Nucleic Acids Res. **36**, 4118 (2008).
[10] C. Kleinschmidt, K. Tovar, W. Hillen, and D. Porschke, Biochemistry **27**, 1094 (1988).
[11] S. E. Halford, Biochem. Soc. Trans. **37**, 343 (2009).
[12] M. von Smoluchowski, Z. Phys. Chem. **92**, 124 (1917).
[13] M. Slutsky and L. A. Mirny, Biophys. J. **87**, 4021 (2004).
[14] M. A. Lomholt, T. Ambjornsson, and R. Metzler, Phys. Rev. Lett. **95**, 260603 (2005).
[15] A. G. Cherstvy, A. B. Kolomeisky, and A. A. Kornyshev, J. Phys. Chem. B **112**, 4741 (2008).
[16] A. M. Florescu and M. Joyeux, J. Chem. Phys. **130**, 015103 (2009).
[17] M. A. Lomholt, B. van den Broek, S. M. J. Kalisch, G. J. L. Wuite, and R. Metzler, Proc. Natl. Acad. Sci. U.S.A. **106**, 8204 (2009).
[18] G. Wilemski and M. Fixman, J. Chem. Phys. **60**, 866 (1974).
[19] G. Wilemski and M. Fixman, J. Chem. Phys. **60**, 878 (1974).
[20] A. Szabo, K. Schulten, and Z. Schulten, J. Chem. Phys. **72**, 4350 (1980).
[21] O. G. Berg, Biopolymers **23**, 1869 (1984).
[22] F. C. Collins and G. E. Kimball, J. Colloid Sci. **4**, 425 (1949).
[23] G. Wilemski and M. Fixman, J. Chem. Phys. **58**, 4009 (1973).
[24] D. R. Cox, Renewal Theory (Methuen, London, 1962).
[25] N. G. van Kampen, Stochastic Processes in Physics and Chemistry, 3rd ed. (Elsevier, Amsterdam, 2007).
[26] A. E. Likthman and C. M. Marques, Europhys. Lett. **75**, 971 (2006).
[27] C. Eun, J. H. Kim, J. Lee, J. H. Bae, Y. R. Lim, S. Lee, and J. Sung, J. Phys. Chem. B **111**, 10468 (2007).
[28] M. Galassi, J. Davies, J. Theiler, B. Gough, G. Jungman, M. Booth, and F. Rossi, GNU Scientific Library Reference Manual, 3rd ed. (Network Theory Ltd., Bristol, UK, 2003).
[29] M. Hinczewski, X. Schlagberger, M. Rubinstein, O. Krichevsky, and R. R. Netz, Macromolecules **42**, 860 (2009).
[30] E. P. Petrov, T. Ohrt, R. G. Winkler, and P. Schwille, Phys. Rev. Lett. **97**, 258101 (2006).
[31] M. Hinczewski and R. R. Netz, Europhys. Lett. **88**, 18001 (2009).

[32] D. L. Ermak and J. A. McCammon, J. Chem. Phys. **69**, 1352 (1978).

[33] J. Rotne and S. Prager, J. Chem. Phys. **50**, 4831 (1969).

[34] H. Yamakawa, J. Chem. Phys. **53**, 436 (1970).

[35] P. H. von Hippel and O. G. Berg, J. Biol. Chem. **264**, 675 (1989).

[36] H. L. Friedman, J. Phys. Chem. **70**, 3931 (1966).

[37] J. M. Deutch and W. Felderhof, J. Chem. Phys. **59**, 1669 (1973).

[38] P. G. Wolynes and J. M. Deutch, J. Chem. Phys. **65**, 450 (1976).

[39] Y. S. Polikanov, V. A. Bondarenko, V. Tchernaenko, Y. I. Jiang, L. C. Lutter, A. Vologodskii, and V. M. Studitsky, Biophys. J. **93**, 2726 (2007).

[40] L. E. Catto, S. R. W. Bellamy, S. E. Retter, and S. E. Halford, Nucleic Acids Res. **36**, 5122 (2008).

[41] K. Šolc and W. Stockmayer, J. Chem. Phys. **54**, 2981 (1971).

[42] D. Shoup, G. Lipari, and A. Szabo, Biophys. J. **36**, 697 (1981).

[43] S. H. Northrup, S. A. Allison, and J. A. McCammon, J. Chem. Phys. **80**, 1517 (1984).

[44] O. Kratky and G. Porod, Recl. Trav. Chim. Pays-Bas **68**, 1106 (1949).

[45] R. G. Winkler, P. Reineker, and L. Harnau, J. Chem. Phys. **101**, 8119 (1994).

[46] B. Y. Ha and D. Thirumalai, J. Chem. Phys. **103**, 9408 (1995).

[47] L. Harnau, R. G. Winkler, and P. Reineker, J. Chem. Phys. **104**, 6355 (1996).

[48] B. H. Zimm, J. Chem. Phys. **24**, 269 (1956).

[49] M. Doi and S. F. Edwards, *The Theory of Polymer Dynamics* (Oxford University Press, Oxford, 1988).